

Effect of hydrogen bond site on proton irradiation of guanine-cytosine base pair: A real-time first-principles study

Chao-Yi Xue(薛超怡), Zhihua Hu(胡志花), Xin Wang(王欣), Ming-Zi Wang(王明梓), and Hong-Jian Feng(冯宏剑)
Citation: Chin. Phys. B, 2026, 35 (**7**): 073101. DOI: 10.1088/1674-1056/ae118c
http://cpb.iphy.ac.cn; http://iopscience.iop.org/cpb

What follows is a list of articles you may be interested in

Theoretical study on low-lying excited states of B_3 molecule

Mu-Hong Hu(胡木宏), Zhi-Xue Zhao(赵志学), Xin-Yi Li(李馨怡), Li-Dan Xiao(肖利丹), and Bing Yan(闫冰)
Chin. Phys. B, 2026, 35 (**1**): 013102. DOI: 10.1088/1674-1056/adf31d

Theoretical study of electron-impact broadening for highly charged Ar XV ion lines

Chao Wu(吴超), Xiang Gao(高翔), Yu-Hao Zhu(朱宇豪), Xiao-Ying Han(韩小英), Bin Duan(段斌),Ju Meng(孟举), Song-Bin Zhang(张松斌), Jun Yan(颜君), Yong Wu(吴勇), and Jian-Guo Wang(王建国)
Chin. Phys. B, 2023, 32 (**5**): 053101. DOI: 10.1088/1674-1056/acb769

Chemical bonding in representative astrophysically relevant neutral, cation, and anion HC_nH chains

Ioan Baldea
Chin. Phys. B, 2022, 31 (**12**): 123101. DOI: 10.1088/1674-1056/ac9b04

Theoretical study on the transition properties of AlF

Yun-Guang Zhang(张云光), Ling-Ling Ji(吉玲玲), Ru Cai(蔡茹),Cong-Ying Zhang(张聪颖), and Jian-Gang Xu(徐建刚)
Chin. Phys. B, 2022, 31 (**5**): 053101. DOI: 10.1088/1674-1056/ac3648

Complex coordinate rotation method based on gradient optimization

Zhi-Da Bai(白志达), Zhen-Xiang Zhong(钟振祥), Zong-Chao Yan(严宗朝), and Ting-Yun Shi(史庭云)
Chin. Phys. B, 2021, 30 (**2**): 023101. DOI: 10.1088/1674-1056/abc156

Effect of hydrogen bond site on proton irradiation of guanine–cytosine base pair: A real-time first-principles study

Chao-Yi Xue(薛超怡)[1,†], Zhihua Hu(胡志花)[1,†], Xin Wang(王欣)[2,‡], Ming-Zi Wang(王明梓)[1,§], and Hong-Jian Feng(冯宏剑)[1]

[1] *School of Physics, Northwest University, Xi'an* 710127, *China*
[2] *School of Physics and Electrical Engineering, Weinan Normal University, Weinan* 714099, *China*

(Received 7 June 2025; revised manuscript received 22 September 2025; accepted manuscript online 10 October 2025)

Ion beam irradiation is widely used in radiotherapy and radiation protection. Investigating hydrogen bond site effects on DNA ionization under proton irradiation is crucial for understanding DNA damage mechanisms. We use real-time time-dependent density functional theory (rt-TDDFT) to establish guanine–cytosine (GC) base pair models and investigate their ionization damage processes under proton irradiation with different hydrogen bond positions in this study. By tracking the deposition energy, electronic stopping power (ESP), atomic forces, charge density, and excited electrons, we explore the impact of hydrogen bond positions on GC base pair ionization damage. The analysis indicates that, compared with the configurations of hydrogen bonds, the hydrogen bond donor (cytosine for LHB, guanine for MHB and RHB) cannot be ignored. Our findings offer important insights into the ionization mechanism and damage processes of DNA molecules during ion beam irradiation, which can guide applications in radiotherapy and radiation protection.

Keywords: proton irradiation, time-dependent density-functional theory, electronic stopping power, charge population

PACS: 31.10.+z, 34.50.Bw, 25.40.Lw

DOI: 10.1088/1674-1056/ae118c **CSTR:** 32038.14.CPB.ae118c

1. Introduction

In recent years, ion beam therapy has been increasingly seen as a pivotal medical technology widely employed in the field of cancer treatment.[1–5] Throughout this process, DNA undergoes irradiation by ion beams, initiating a series of intricate biophysical and chemical reactions.[6–8] The direct and indirect damage of DNA exerts a considerable influence on determining the survival or demise of cells.[9,10] Direct ionization can result in critical bond breakages within DNA, for instance, the breaking of base pairs or more significant alterations to the sugar-phosphate backbone.[11–15] On the other hand, indirect effects refer to damage induced by the interaction between DNA and the products of the decomposition of water molecules by radiation, which include free radicals and other reactive species, including hydroxyl radicals, singlet oxygen, and hydrogen peroxide.[16–18] Therefore, a profound investigation into the microscopic interactions between ion beams and DNA holds significant implications for understanding the radiation-induced cell death processes and improving the efficacy of ion beam therapy.

In previous studies, real-time time-dependent density functional theory (rt-TDDFT) has been extensively utilized to simulate the ion beam-induced electronic excitation dynamics for DNA.[19–29] A groundbreaking rt-TDDFT simulation had recently been reported by Yost and colleagues,[22] focusing on collisions between the proton and α particle with a DNA double strand. Seraide and collaborators investigated the radiation damage caused by proton collisions at low velocities with hydrogen bonds and phosphate groups separately.[23] Their findings indicated that a proton at a velocity of 0.4 a.u. (in atomic unit) collides with hydrogen bond led to base damage while keeping the backbone intact. In addition, some studies analyze how variations in collision sites, collision orientations, and the energy of protons incident at low energy affect the collision dynamics of cytosine.[24,25] However, there is a scarcity of first-principles studies on the ionization damage to DNA caused by proton irradiation with respect to the positions of hydrogen bonds.

Hydrogen bonds maintain the correct pairing of base pairs and the overall structural integrity. Ionization damage near the hydrogen bond leads to a change in local structure and then destroys the integrity of DNA. It is therefore critical to explore the proton-induced ionization damage at hydrogen-bond sites of DNA. This study systematically investigates the ionizing radiation damage of the guanine–cytosine (GC) base pair caused by proton irradiation at different incident velocities and hydrogen-bond sites. The aim is to understand how the positions and velocities of the proton affect the ionization damage.

[†]These authors contributed equally to this work.
[‡]Corresponding author. E-mail: wangx@wnu.edu.cn
[§]Corresponding author. E-mail: mzwang@nwu.edu.cn

© 2026 Chinese Physical Society and IOP Publishing Ltd. All rights, including for text and data mining, AI training, and similar technologies, are reserved.

The findings of this study strengthen the comprehensive understanding of the micro-interactions between ion beams and DNA, which not only provides theoretical insights for improving treatment targeting, but also offers guidance on optimizing therapeutic doses and reducing side effects during radiation therapy.

In this study, utilizing rt-TDDFT, we constructed a model of proton irradiation on the GC base pair and simulated the irradiation process under varying incident velocities (ranging from 0.5 a.u. to 6.0 a.u.) and incident positions. By tracking energy deposition, electronic stopping power (ESP), atomic force, charge density, and the time evolution of excited states, we deeply analyzed the ionization damage process under proton irradiation. In our previous studies, we also applied the same methodology to investigate the microscopic mechanisms of low-energy proton irradiation on normal and mutant DNA,[20] and the impact of carbon ion irradiation on thionine and DNA.[27] The outcomes of this research enhance the overall understanding of the microscopic interactions between ion beams and DNA, offering guidance for the empirical evaluation of potential radiation dangers, optimization of radiotherapy protocols, and the development of radiation protection strategies.

2. Computational models and details

In the paper, we establish a GC base pair containing 69 host atoms as the target material.[20] H atoms are added to the O3′ and O5′ ends of the model to saturate the electrons and achieve a stable structure. Figures 1(a) and 1(b) illustrate the top and side views of a GC base pair structure, respectively. For clarity in description, the three hydrogen bonds (H-bonds) of the GC base pair: O[G]–H[C], H[G]–N[C], and H[G]–O[C] chemical bonds are described as the left hydrogen bond (LHB), middle hydrogen bond (MHB) and right hydrogen bond (RHB), respectively. The hydrogen bond donor for the LHB is the cytosine base, and the hydrogen bond donor for the MHB and RHB is the guanine base. The positions indicated by the blue boxes in Figs. 1(c)–1(e) represent different hydrogen bond locations respectively. The GC base pair holds a 15-Å vacuum layer in all three directions. Subsequently, a mathematical expression for the total energy in terms of volume is calculated to determine a stable structure for further calculations, as illustrated in Fig. S1 in supporting material. Two O3′ atoms and two O5′ atoms at the end of the model are fixed to simulate the binding effect with adjacent base pairs in the whole process. Although the π–π interactions between base pairs and variations in DNA sequence are secondary contributors to DNA damage, base pairs are the fundamental units of DNA, and the interaction between atoms within the base pair and projectiles is the most crucial factor influencing the energy deposition process. To justify the validity of using a single GC base pair simplified model, a poly(G)–poly(C) double-strand model consisting of five GC base pairs is constructed, and the energy deposition process of the poly(G)–poly(C) double strand under proton irradiation at 6 a.u. is simulated, as shown in Fig. S2. Figures S2(c) and S2(d), which indicate that the energy deposition process shows a simple superposition of the single base pair. Therefore, the single GC base pair can significantly reflect trends in the microscopic mechanism changes of the DNA model under proton irradiation.

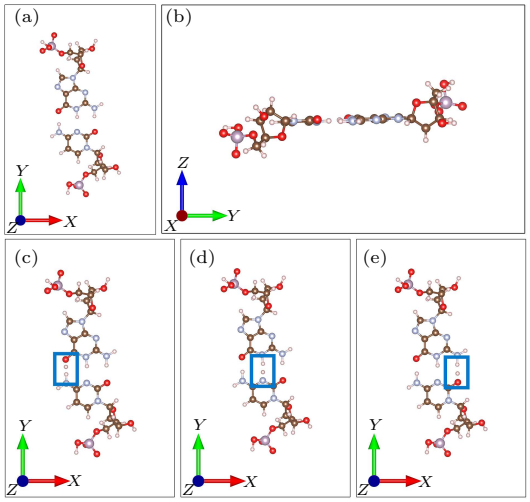


Fig. 1. (a) Top viewport of a GC base pair, (b) side view of a GC base pair, (c) top view of the model with proton irradiation along (c) LHB, (d) MHB, (e) RHB.

The entire calculation process is carried out using the TDDFT module within the Spanish Initiative for electronic simulations with thousands of atoms (SIESTA) code,[30–33] aimed at analyzing the microscopic physical process of proton irradiation on the GC base pair. And a proton is placed 15 Å from the base pair cross-section to simulate proton irradiation on the base pair. The computational procedure comprises two primary phases. Initially, the ground state attributes of the model are obtained by employing density functional theory.[34,35] The obtained ground-state wave function is then used as the initial configuration for subsequent TDDFT simulation.[36,37] During the calculations, to determine the appropriate parameters for the system, we first assessed the total energy of a GC base pair under various parameter conditions, including exchange–correlation functional, basis sets, cutoff energy, K-points, and mixing weight,[38,39] as presented in supporting material Table S1 and Figs. 2(a) and 2(b). The test analysis suggests that: (i) when the mixing weight of 0.02 and the K-point grid parameters of $1 \times 1 \times 1$ are selected, the system energy value of the ground state obtained by the double zeta plus polarization (DZP) basis set is -11953.4 eV, and the triple zeta plus polarization (TZP) basis set is -11955.9 eV, both DZP and TZP basis sets yield relatively low system energies, indicating that both basis sets can accurately describe the

electronic states of the model. While the computational time required when using the TZP is nearly twice that of the DZP; (ii) when the DZP basis set and the K-point grid parameters of $1 \times 1 \times 1$ are selected, the influence of different mixed weights on the total energy is below 10^{-4} eV, which can be ignored; (iii) when the DZP basis set and the mixing weight of 0.02 parameters are selected, different K-point grids have no effect on the total energy value; (iv) total energy tends to be stable at 400 Ry with the increase of cutoff energy (Fig. 2(a)); (v) the electronic energy deposition obtained using local density approximation (LDA) and generalized gradient approximation (GGA) in the Perdew–Burke–Emzerhof (PBE) form during the proton irradiation of the MHB (Fig. 2(b)), indicates that the differences between the two are minimal. Therefore, to balance computational efficiency and accuracy, the subsequent calculations employed the DZP basis set, a mixing weight of 0.2, a K-point grid of $1 \times 1 \times 1$, a cutoff energy of 400 Ry, and the LDA method. Secondly, the simulation process of ion irradiation base pair is performed using TDDFT theory, where the proton with certain initial velocities moves along a specified trajectory at a time step of 0.002 fs through the base pair, the proton velocity is much greater than the vibration rate of the GC base pair atoms. When the proton passes through different H-bond positions, it does not collide with the nuclei of atoms near the channel but undergoes inelastic collisions with electrons near the nuclei. Time-resolved physical quantities including system energy, atomic force, electronic eigenvalues, charge population, and charge density can be extracted from dynamic simulation trajectories.[40–43]

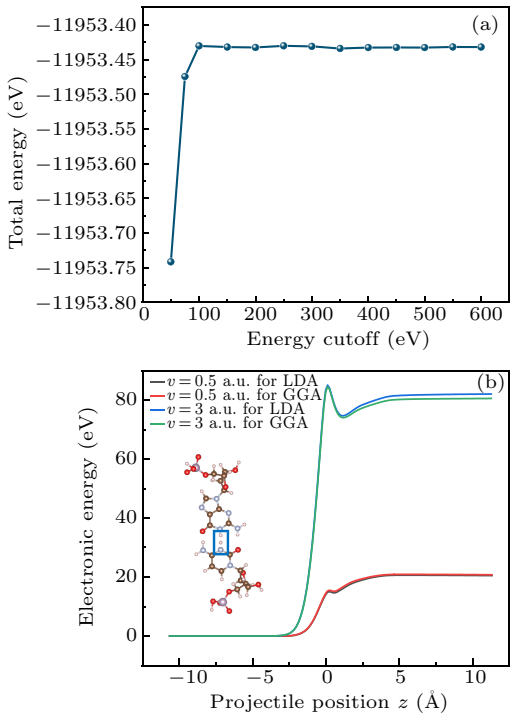


Fig. 2. (a) Total energy as a function of energy cutoff. (b) Electronic energy as a mathematical relationship of proton positions as the proton passing the MHB with 0.5 a.u. and 3 a.u.

3. Results and discussion

Figure 3 is the electronic energy (E_{ks}) when the proton irradiates different H-bonds along the Z direction of the base pair. The abscissa value represents the distance from the base pair cross-section, and the coordinate origin represents the location of the cross-section. From the electronic energy in Fig. 3, it is clear that the electronic trend for H-bonds with a different intruding position of the proton is the same while exhibiting increases to varying extents. The same trend is as follows: the proton does not deposit energy until it reaches a certain distance from the cross-section. This shows that the energy deposition progression is critically determined by the environment around the invasive channel. When the intruding proton's velocity is 0.5 a.u., electronic energy starts increasing when the proton is at 1.8 Å before the base-pair center, while starting at a distance of about 2.8 Å for 6.0 a.u. With an increase in velocity, the distance between the proton and the cross-section of the base pair increases when the electronic energy deposition by the proton begins. The instantaneous physical properties exhibit a significant reliance on the intrusion path and velocity. When the intruded ion has a small velocity, the electronic energy deposition needs to occur closer to the target atoms.

Figure 3 demonstrates that the electronic energy deposition, when the proton is at the position of the cross-section, increases with velocity, as shown in Fig. S3, which presents the electronic energy deposition values when the proton is at the position of the cross-section at different velocities. When the proton speed exceeds 2.5 a.u., the electronic energy deposition reaches a maximum over the entire process. This demonstrates that when the intruding ion has a higher intruding velocity, enhanced ion-target interactions lead to higher electronic energy, increased deposition rates, stronger inter-atomic interactions, and a greater number of excited electrons.[20] Within the distance from 0 Å to 1.5 Å after the proton passes through the cross-section, the electronic energy deposition shows a decreasing trend, indicating that the charge just excited is extremely unstable and back-flow occurs; an excitation decay process occurs, and the extent of de-excitation strengthens as the penetration velocity increases. When the proton reaches a position at a distance of 1.5 Å after the cross-section, the electronic energy deposition increases slightly as the proton moves away until it stabilizes once the proton reaches a position at a distance of 4.5 Å after the cross-section. It shows that there is a secondary excitation for the ground-state electrons, which could be attributed to the attenuation of excited charge. The final electronic energy deposition is the value that tends to stabilize. For different H-bonds, the final electronic energy deposition reaches a maximum when the proton velocity is 3 a.u. as shown in Fig. 3.

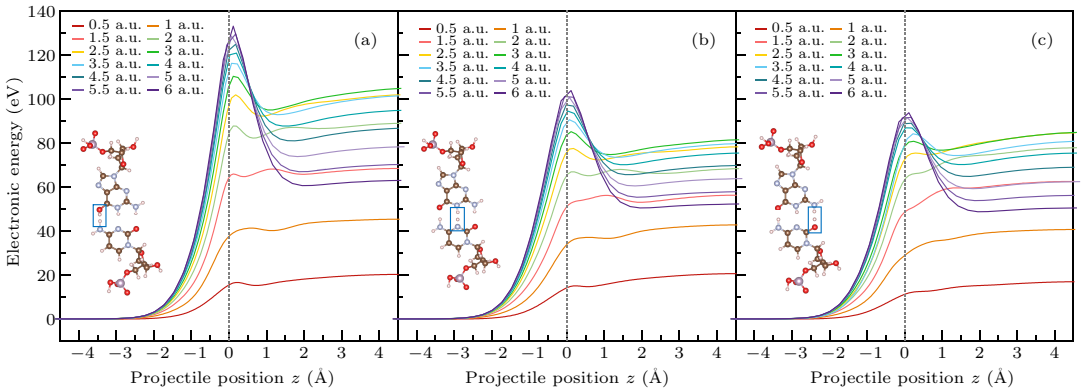


Fig. 3. Electronic energy E_{ks} as a function of the proton position for the proton at 0.5 a.u.–6 a.u. passing through (a) LHB, (b) MHB, and (c) RHB. The insets show the intruding position of proton passing through the H-bonds. The red points represent the electronic energy deposition values when the proton is at the position of the cross-section.

To further illustrate the electron excitation and excitation decay process with the velocity of an intruding proton, the instantaneous electronic stopping power (ESP), a derivative of energy concerning proton movement distance $\mathrm{d}E_{\mathrm{ks}}/\mathrm{d}x$ as shown in Fig. 4. The instantaneous ESP value greater than zero indicates the excitation process, while less than zero means the excitation decay process. It can be seen from Fig. 4 that there is an obvious excitation and excitation decay process when the proton irradiates H-bonds with a speed exceeding 3 a.u. For all H-bonds, the electron starts to be excited closing to the 2.8 Å before the cross-section, which aligns with the previous data. After the proton passes through the cross-section, the electrons excited have an excitation decay process due to the energy instability, until completed at 3.0 Å away from the cross-section. Meanwhile, when the velocity is greater than 3 a.u., the electron excitation and excitation decay extent are strengthened with the increase in intruding velocity. When the speed is 1 a.u. and 2 a.u., the excitation decay process is different with the H-bonds position. For LHB, both 1 a.u. and 2 a.u. have an excitation decay process and a secondary excitation, as shown in Fig. 4(a). When the proton passes through the MHB, there is no excitation decay at 1 a.u. and the same as LHB for 2 a.u. as depicted in Fig. 4(b). From the data, the data indicates that for RHB as shown in Fig. 4(c), there is no excitation decay either 1 a.u. nor 2 a.u. It may be caused by the longer reaction time of the excitation and excitation decay process for low-energy proton.

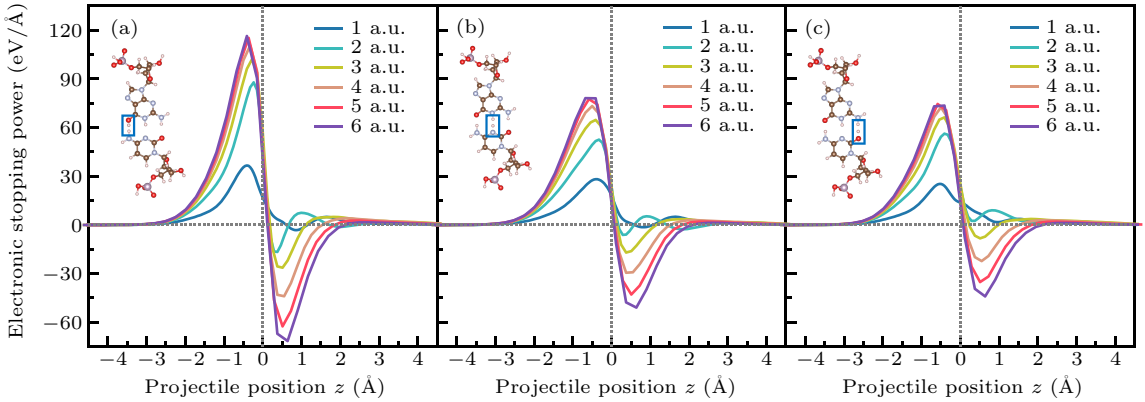


Fig. 4. The instantaneous electronic stopping power (ESP) as a function of proton position under proton passing (a) LHB, (b) MHB, (c) RHB. with the velocity of 1 a.u.–6 a.u. The red points represent the maximum instantaneous electronic stopping power values.

The relationship between the ESP and the intruding velocity (0.5 a.u.–6 a.u.) is shown in Fig. 5, during the process of the proton moving from 4.5 Å before to 4.5 Å after the cross-section. It can be seen that (i) when the velocity of the proton is 0.5 a.u. and 1 a.u., the kinetic energy of the proton is limited, rendering it insufficient to effectively excite the electron cloud. The ESP for different H-bonds is not much different; (ii) when the velocity of the proton is between 1.5 a.u. and 3.5 a.u., the interaction between the projectile and the electron cloud leads to the excitation or ionization of the target atom, accompanied by a notable de-excitation or energy back-flow process. The ESP reaches a maximum value when the proton's speed is 3 a.u., but the relationship between the ESP and the position shows the following trend: LHB>RHB>MHB. To further investigate the differences between various hydrogen bond sites during irradiation, we compared the energy deposition process of the proton with velocities of 2.5 a.u., 3 a.u., and 3.5 a.u. at different irradiation sites, as shown in Fig. 6. Figures 6(a) and 6(b) illustrate that during the energy deposition process of irradiating MHB and RHB, the electronic energy

deposition decreases after the proton passes through the base pair cross-section, indicating that the just-excited charge is extremely unstable, back-flow occurs, and an excitation decay process of the excited charge exists. The hydrogen bond acceptor for MHB is the N atom on the cytosine base, while the hydrogen bond acceptor for RHB is the O atom on the cytosine base; the N atom has a relatively high first ionization energy, which shows that its valence electrons are more tightly bound and the spatial distribution of electron clouds is more concentrated. This strong binding results in higher initial energy deposition at the cross-section for MHB compared to RHB. However, the stability of these tightly bound electronic states is poor, which makes the excited electrons fall back quickly through non-radiative relaxation. This results in a portion of the initial deposited energy being released through radiation or secondary electrons. Therefore, the effective energy of MHB is reduced more than that of RHB in this velocity range, resulting in the ESP values for MHB being lower than the ESP values for RHB. (iii) When the velocity of the proton is greater than 3.5 a.u., the ESP for different H-bonds decreases with the increase of the velocity. In the meantime, the ESP for LHB is still the largest, while the values of RHB and MHB are not much different, as shown in Fig. 6(b). Under high velocity conditions, the interaction time between the proton and the electron cloud is significantly reduced, making it difficult for the excited states to undergo relaxation promptly. Thus, the de-excitation mechanism characteristic of the medium velocity range is no longer predominant. The deposition energy primarily depends on the overall electron density distribution of the base pair. Since the hydrogen bond donors for both MHB and RHB are cytosine bases, the local electron density differences become negligible, leading to the convergence of their ESP curves. People usually focus on the difference between O–H and N–H for H-bonds, but the difference between LHB and RHB deserves more attention. To further study this differentiation among the H-bond positions, we also analyzed the drag force during the proton movement exerted by the base pair.

Compared to the study by Yost *et al.*,[22] the influence of proton velocity on electronic energy deposition is more pronounced when protons irradiate different hydrogen-bond sites. This discrepancy can be attributed to several factors: (i) The selected projectile trajectories are different, which results in varying electron densities within the channels. Our study primarily investigates radiation damage caused by proton irradiation along the direction perpendicular to the base-pair cross-section, where the incident ions interact with electrons near the hydrogen-bond sites. In contrast, Yost *et al.* focused on radiation damage when the ion passed through the space between two base pairs along a direction parallel to the base cross-section, where the incident ions interact with the π-electron cloud. Since the hydrogen-bond interactions between connected bases are stronger than the π–π interactions between base pairs, the electron density along our proton trajectory is higher, leading to greater energy deposition. (ii) In Yost *et al.*'s study, the intermolecular π–π interactions impede the backflow of excited electrons during irradiation. However, hydrogen bonds facilitate the transfer of excited electrons, promoting energy transfer,[28] which contributes to greater energy deposition.

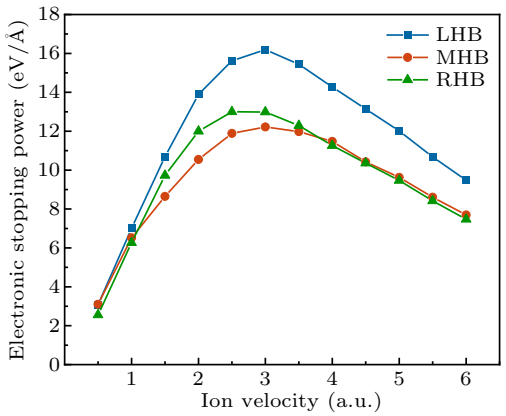


Fig. 5. The mathematical association between electron stopping power (ESP) and irradiation velocity (0.5 a.u.–6 a.u.) when the proton passes (a) LHB, (b) MHB, (c) RHB.

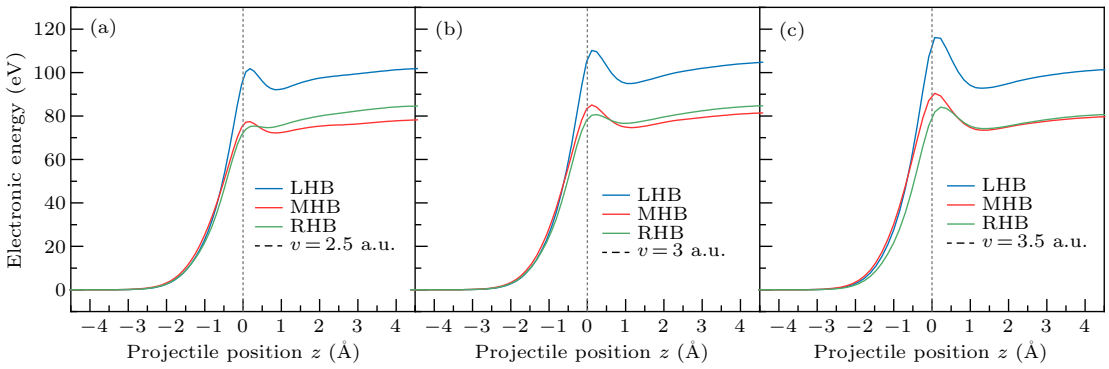


Fig. 6. Electronic energy E_{ks} as a function of the proton position for the proton at (a) 2.5 a.u., (b) 3 a.u., and (c) 3.5 a.u. passing through the LHB, MHB, and RHB.

Figure 7 shows the change of the proton force along the three axes for an intruding proton at a velocity of 3.0 a.u. as it passes through the H-bonds. For H-bonds at any position, the proton starts to experience the atomic force when it is at a distance of 2.8 Å before the base pair cross-section, indicating that the energy begins to be deposited at this time, and the proton is not stressed until it is at a distance of 2.5 Å after the cross-section. In the Z direction, the proton experiences resistance opposite to the incident direction at any position, and the resistance is maximum when near the base pair cross-section. For the Y direction, the force is directed downward from guanine to cytosine when the proton passes through the LHB, while the force is opposite, from cytosine to guanine, when it passes the MHB and RHB. When the proton passes through the cross-section, it is forced toward the hydrogen bond donor and experiences the maximal force. The proton moves toward the hydrogen bond donor along the Y-direction during the irradiation process at different H-bond sites. Combined with the force distributions along Z and Y axes, the peak energy deposition near the cross-section is consistent with the results in Fig. 3. Compared with the Z and Y orientations, the magnitude of the force in the X-direction does not change significantly, but the direction can be judged. When the proton passes through the LHB, the force is directed to the negative orientation of the X-direction, while the force is directed to the positive orientation of the X-direction when it passes the MHB and RHB.

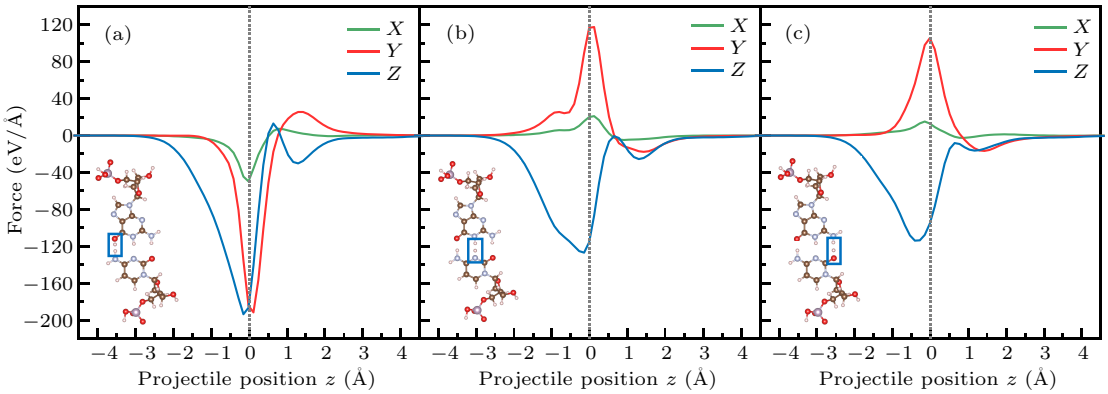


Fig. 7. The change of the proton force along the three axes for an intruding proton at a velocity of 3.0 a.u. as it passes through (a) LHB, (b) MHB, (c) RHB. The positive directions of the X and Y directions are illustrated in Fig. 1(a), and the positive direction of the Z direction is illustrated in Fig. 1(b). The insets show the intruding position of proton passing H-bonds.

Through the analysis of the charge fluctuations in the proton and atoms within the material being targeted, the findings show that the charges of the proton and atoms near the channel have changed significantly during proton irradiation. Figure 8 illustrates the charge fluctuations of atoms surrounding the channel and each molecular fragment of the base pair for the intruding proton with 3.0 a.u. From Fig. 8(a), it can be observed that when the proton passes LHB, strong electron excitation occurs when the proton almost reaches the cross-section. The O1 and H2 atoms lose electrons and generate a large number of holes. At the same time, the proton captures numerous excited electrons, leading to both the guanine and cytosine bases being in an electron-deficient state as shown in Fig. 8(d). Within the distance of 0 to 3.8 Å after the proton passes through the cross-section, the excited electrons decay rapidly and there is an excitation decay process. The electrons captured by the proton flow back around the O1 and H2 atoms. The O1 atom retains an electron-deficient configuration, leading to the guanine base being oxidized, while the cytosine base holds an electron-enriched configuration due to the increasing electron density around the H2 atom. During the movement of the proton from 3.8 Å to further positions after passing through the cross-section, the electrons captured by the proton tend to stabilize, and the proton takes away about 0.9 electrons from the base pair. There exists a dynamical electron equilibrium process within the base pair. The electron levels of the guanine base gradually increase, while those of the cytosine base slowly diminish, indicating that the cytosine base undergoes electron transfer to the guanine base. When the proton irradiates MHB and RHB, the charge fluctuation trend of atoms near the channel is similar to that of LHB. The total charge of each molecular fragment mainly depends on the charge of atoms near the channel, as shown in Figs. 8(b)–8(c) and 8(e)–8(f). Finally, the proton captures some electrons, and the number of captured electrons follows the pattern: LHB>MHB>RHB. The N4 and O6 atoms are in an electron-deficient state, while the H3 and H5 atoms are in an electron-rich state. The situation of charge fluctuations on each molecular fragment is the opposite. During the movement of the proton from 3.8 Å to further positions after passing through the cross-section, the guanine base undergoes electron transfer to the cytosine base.

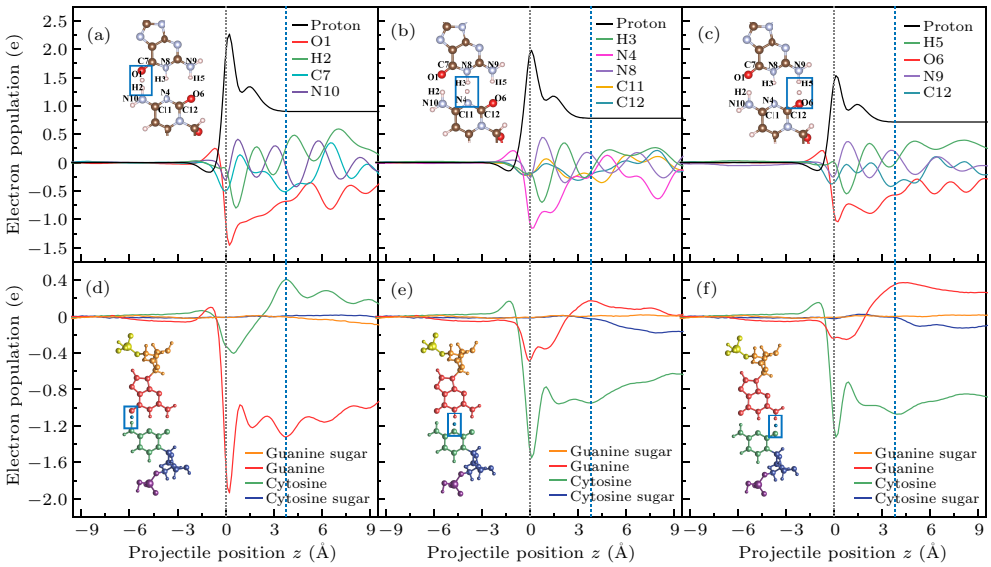


Fig. 8. Charge fluctuations on atoms surrounding the channel for the intruding proton at 3.0 a.u. passes through (a) LHB, (b) MHB, and (c) RHB. The insets show the atomic number. Charge fluctuations on each molecular fragment of the base pair for the intruding proton with 3.0 a.u. passes through (d) LHB, (e) MHB, and (f) RHB. The gray and blue dashed lines represent the positions of the proton at cross-section and at a distance of 3.8 Å away from the cross-section, respectively. The insets illustrate the spatial arrangement of C–G base pair. Color coding: red represents guanine, orange is used for the guanine sugar, green represents cytosine and blue for the cytosine sugar.

To further discuss the change of charge density distribution of the base pair caused by proton irradiation at different H-bond positions, Fig. 9 shows the charge density change discrepancy measured at 6.0 Å after the cross-section for the intruding proton at 3.0 a.u. passes through the H-bonds. At that moment, a dynamical equilibrium process is established for the electrons in the base pair, originating from the overlap of secondarily excited electrons and polarization-driven electrons in oscillation induced by the atomic vibrations.[20] When the proton passes through the LHB as shown in Fig. 9(a), guanine is in a state of electron deficiency because the holes are mainly located in the oxygen atom near the channel, while the cytosine is in a state of electron abundance because the electrons are mainly distributed around the hydrogen atom near the channel as indicated in Figs. 9(b) and 9(c). After the proton passes through the MHB and RHB, the charge distribution on each molecular fragment is opposite. The electrons are mainly located in the hydrogen atoms near the channel, making guanine in an electron-enriched configuration. The reason why cytosine is in an electron-deficient configuration is different: for MHB, the holes are mainly distributed around the nitrogen atom near the channel, while for RHB they are around the oxygen atom. The current research on irradiated hydrogen bonds mainly focuses on the configurations.[25] Our research results show that the hydrogen bond donor (cytosine for LHB, and guanine for MHB and RHB) cannot be ignored.

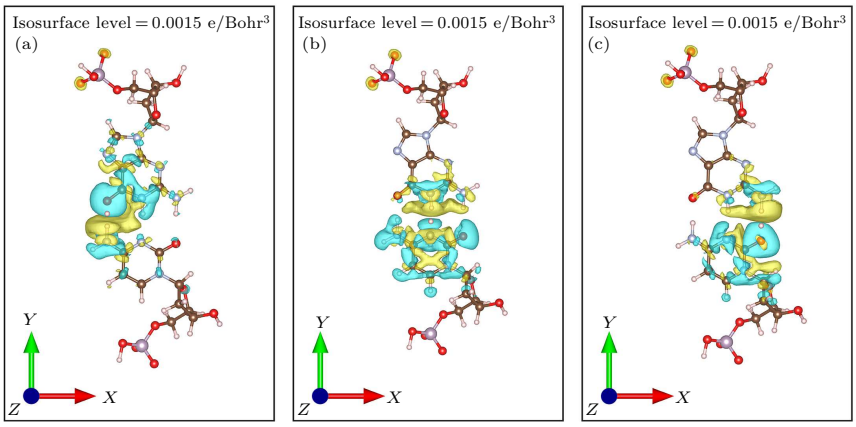


Fig. 9. The charge density change difference at 6.0 Å away from the cross-section for the proton irradiation with 3.0 a.u. passing (a) LHB, (b) MHB, (c) RHB. Color code: positive in blue, negative in yellow.

4. Conclusion

In summary, based on the TDDFT theoretical framework, our study focused on the time evolution of electronic deposition energy, electronic stopping power (ESP), atom forces, excited electron, and charge density of base pair for the proton for velocities from 0.5 a.u. to 6 a.u. passes the H-bonds at different positions. The study indicates that proton velocity and hydrogen bond position significantly affect the ionization

damage of GC base pairs, with the largest electronic energy deposition at the LHB. This can be attributed to the differences in hydrogen bond donors. This distinction originates from different hydrogen bond donors. Although LHB and RHB are O–H hydrogen bonds while MHB is an N–H bond, our results prove that hydrogen bond donors exert a more dominant effect than bond geometric configurations and cannot be neglected. Since the hydrogen bond donor connecting the hydrogen atom for LHB is cytosine, the guanine is always in a state of electron deficiency after proton irradiation. During the movement of the proton from 3.8 Å to further positions after passing through the cross-section, there is an electron transfer from cytosine to guanine. For MHB and RHB, the guanine is in an electron-enriched configuration because of the different hydrogen bond donor, causing the flow of electrons in the opposite direction from guanine to cytosine. The ESP shows that the maximum electronic energy deposition occurs when the proton is at 3 a.u. for all H-bonds. Future research could systematically explore the ionization behavior of DNA under proton irradiation at different chemical bond sites, thereby deepening the understanding of the ionization damage mechanisms, and through multidimensional studies of ionization damage under various conditions, providing a theoretical basis for quantitatively assessing radiation risks, optimizing radiation treatment plans, and developing radiation protection strategies.

Acknowledgements

Project supported by the National Natural Science Foundation of China (Grant No. 11904286) and the Scientific Research Program Funded by Science and Technology Department of Shaanxi Province, China (Grant No. 2024JC-YBQN-0045).

References

[1] Verkhovtsev A, Surdutovich E and Solov'yov A V 2016 *Sci. Rep.* **6** 27654
[2] Durante M and Loeffler J S 2009 *Nature Reviews Clinical Oncology* **7** 37
[3] Dong Y, Liao H, Gao Y, Cloutier P, Zheng Y and Sanche L 2021 *J. Phys. Chem. Lett.* **12** 717
[4] Baskar R, Lee K A, Yeo R and Yeoh K W 2012 *International Journal of Medical Sciences* **9** 193
[5] Matsuya Y, Kai T, Parisi A, Yoshii Y and Sato T 2022 *Physics in Medicine & Biology* **67** 215017
[6] Nikjoo H, O'Neill P, Terrissol M and Goodhead D 1994 *International Journal of Radiation Biology* **66** 453
[7] Friedland W, Dingfelder M, Kundrát P and Jacob P 2011 *Mutation ResearchFundamental and Molecular Mechanisms of Mutagenesis* **711** 28
[8] Hutchinson F 1985 *Progress in Nucleic Acid Research and Molecular Biology* **32** 115
[9] Alizadeh E, Orlando T M and Sanche L 2015 *Ann. Rev. Phys. Chem.* **66** 379
[10] Barrios R, Skurski P and Simons J 2002 *J. Phys. Chem. B* **106** 7991
[11] Surdutovich E and Solov'yov A V 2014 *Eur. Phys. J. D* **68** 1
[12] Souici M, Khalil T T, Muller D, Raffy Q, Barillon R, Belafrites A, Champion C and Fromm M 2017 *J. Phys. Chem. B* **121** 497
[13] Ushigome T, Shikazono N, Fujii K, Watanabe R, Suzuki M, Tsuruoka C, Tauchi H and Yokoya A 2012 *Radiation Research* **177** 614
[14] Bhaskaran R and Sarma M 2015 *J. Phys. Chem. A* **119** 10130
[15] Deng Z, Bald I, Illenberger E and Huels M A 2005 *Phys. Rev. Lett.* **95** 153201
[16] Ribar A, Huber S E, Śmiałek M A, Tanzer K, Neustetter M, Schürmann R, Bald I and Denifl S 2018 *Phys. Chem. Chem. Phys.* **20** 5578
[17] Kumar A and Sevilla M D 2010 *Chem. Rev.* **110** 7002
[18] Pachnerová Brabcová K, Štěpán V, Karamitros M, Karabín M, Dostálek P, Incerti S, Davídková M and Sihver L 2015 *Radiation Protection Dosimetry* **166** 44
[19] Khalili F, Vafaee M and Shokri B 2021 *Phys. Chem. Chem. Phys.* **23** 23005
[20] Deng Z Y, Hu Z and Feng H J 2022 *Appl. Phys. Lett.* **120** 043702
[21] Yost D C, Yao Y and Kanai Y 2019 *J. Phys. Chem. Lett.* **11** 229
[22] Yost D C and Kanai Y 2019 *J. Am. Chem. Soc.* **141** 5241
[23] Seraide R, Bernal M A, Brunetto G, de Giovannini U and Rubio A 2017 *J. Phys. Chem. B* **121** 7276
[24] Wang Z P, Zhang F S, Xu X F and Qian C Y 2020 *Chin. Phys. B* **29** 023401
[25] Wang X, Wang Z P, Zhang F S and Qian C Y 2022 *Chin. Phys. B* **31** 063401
[26] Hu Z, Deng Z Y and Feng H J 2024 *Phys. Chem. Chem. Phys.* **26** 25363
[27] Deng Z Y, Hu Z and Feng H J 2022 *J. Phys.: Conden. Matter* **51** 025101
[28] Deng Z Y, Hu Z and Feng H J 2023 *Chemical Engineering Journal* **466** 143002
[29] He Y, Deng Z Y and Feng H J 2023 *J. Phys.: Conden. Matter* **35** 415502
[30] Koval P, Barbry M and Sánchez-Portal D 2019 *Comput. Phys. Commun.* **236** 188
[31] Pemmaraju C D, Vila F D, Kas J J, Sato S A, Rehr J J, Yabana K and Prendergast D 2018 *Comput. Phys. Commun.* **226** 30
[32] García A, Papior N, Akhtar A, Artacho E, Blum V, Bosoni E, Brandimarte P, Brandbyge M, Cerdá J I, Corsetti F, Cuadrado R, Dikan V, Ferrer J, Gale J, García-Fernández P, García-Suárez V M, García S, Huhs G, Illera S, Korytár R, Koval P, Lebedeva I, Lin L, López-Tarifa P, Mayo S G, Mohr S, Ordejón P, Postnikov A, Pouillon Y, Pruneda M, Robles R, Sánchez-Portal D, Soler J M, Ullah R, Yu V W Z and Junquera J 2020 *J. Chem. Phys.* **152** 204108
[33] Soler J M, Artacho E, Gale J D, García A, Junquera J, Ordejón P and Sánchez-Portal D 2002 *J. Phys.: Conden. Matter* **14** 2745
[34] Qian Z and Sahni V 1998 *Phys. Rev. A* **57** 2527
[35] Davydov D, Young T D and Steinmann P 2016 *International Journal for Numerical Methods in Engineering* **106** 863
[36] Castro A, Marques M A and Rubio A 2004 *J. Chem. Phys.* **121** 3425
[37] Watanabe N and Tsukada M 2002 *Phys. Rev. E* **65** 036705
[38] Tsolakidis A, Sánchez-Portal D and Martin R M 2002 *Phys. Rev. B* **66** 235416
[39] Mulliken R S 1955 *J. Chem. Phys.* **23** 1833
[40] Correa A A, Kohanoff J, Artacho E, Sánchez-Portal D and Caro A 2012 *Phys. Rev. Lett.* **108** 213201
[41] Hatcher R, Beck M, Tackett A and Pantelides S T 2008 *Phys. Rev. Lett.* **100** 103201
[42] Correa A A 2018 *Comput. Mater. Sci.* **150** 291
[43] Shukri A A, Bruneval F and Reining L 2016 *Phys. Rev. B* **93** 035128